Large-Scale Model for the Dissolution of Heterogeneous Porous Formations: Theory and Numerical Validation

Jianwei Guo, Farid Laouafa, Michel Quintard

Large-Scale Model for the Dissolution of Heterogeneous Porous Formations: Theory and Numerical Validation

Jianwei Guo[1] · Farid Laouafa[2] · Michel Quintard[3]

Abstract

In this paper, we study the dissolution of a porous formation made of soluble and insoluble materials with various types of Darcy-scale heterogeneities. Based on the assumption of scale separations, i.e., the convective and diffusive Damköhler numbers are smaller than certain limits which are documented in the paper, we apply large-scale upscaling to the Darcy-scale model to develop large-scale equations, which are used to describe the dis-solution of porous formations with Darcy-scale heterogeneities. History-dependent clo-sure problems are provided to get the effective parameters in the large-scale model. The large-scale model validity is tested by comparing numerical results for a 1D flow prob-lem in a stratified system and a 2D flow problem in a nodular system to the Darcy-scale ones. The good agreement between results at Darcy and large scales shows the robustness of the large-scale model in representing the Darcy-scale results for the stratified system, even when the dissolution front is very sharp. Large-scale results for the nodular system represent satisfactorily the averaged Darcy-scale behaviors when the dissolution front is relatively thick, i.e., when model assumptions are satisfied, while there may be as expected some discrepancy generated between direct numerical simulations and large-scale results in the case of thin dissolution front. Overall, this study demonstrates the possibility of building a fully homogenized large-scale model incorporating dissolution history effects, and that the resulting large-scale model is capable to catch the main features of the Darcy-scale results within its applicability domain.

- **Large-scale model is developed for the dissolution of heterogeneous porousmedia, taking dissolution history effect into account.**
- **A sequential algorithm is proposed for the solution of effective mass exchange coefficient and effective permeability tensor.**
- **The large-scale model is validated for stratied and nodular systems.**

Keywords Dissolution · Heterogeneous porous media · Large-scale model · Volume averaging

List of Symbols

Roman letters

$\mathbf{b}$	Mapping vector, m
c_{eq}	Thermodynamic equilibrium concentration of the dissolved solid, $\mathrm{kg\,m^{-3}}$
C_l, C_l^*	Darcy- and large-scale intrinsic average concentration of the dissolved solid, respectively, $\mathrm{kg\,m^{-3}}$
$\tilde{C}_l$	Large-scale concentration deviation, $\mathrm{kg\,m^{-3}}$
D	Diameter of the inclusions in the 2D geometry, m
Da, Da_M	Micro- and macroscale Damköhler number, respectively, dimensionless
D_r	Reference diffusion coefficient, $\mathrm{m^2\,s^{-1}}$
$\mathbf{D}_l$	Darcy-scale dispersion tensor, $\mathrm{m^2\,s^{-1}}$
$\mathbf{g}$	Gravitational acceleration, $\mathrm{m\,s^{-2}}$
H	Height of the 2D unit cell, m
K_l	Permeability, $\mathrm{m^2}$
K_0	Permeability constant, $\mathrm{m^2}$
K_s	Mass exchange of the dissolving solid, $\mathrm{kg\,m^{-3}\,s^{-1}}$
$\mathbf{K}_l$, $\mathbf{K}_l^*$	Darcy- and large-scale permeability tensor, respectively, $\mathrm{m^2}$
ℓ_d	Thickness of dissolution front, m
ℓ_h	Characteristic length of heterogeneity, m
ℓ_i, ℓ_l, ℓ_s	Pore-scale characteristic lengths, m
ℓ_ω , ℓ_η	Darcy-scale characteristic length, m
L	Large-scale characteristic length, m
P_l, P_l^*	Darcy- and large-scale intrinsic average pressure, respectively, Pa
P_e	Pressure at the inlet of the 2D nodular system, Pa
Pe_M	Macroscale Péclet number, dimensionless
r_0, R_0	Characteristic length of the REV used to define Darcy- and large-scale variables, respectively, m
$\mathbf{r}$	Position vector, m
S, S^*	Darcy- and large-scale solid mineral saturation, respectively, dimensionless
$\widehat{S}$, $\widehat{S^*}$	Domain average of S and S^*, respectively, dimensionless
$\tilde{S}$	Large-scale soluble solid saturation deviation, dimensionless
t	time, s
U_r	Reference velocity, $\mathrm{m\,s^{-1}}$
$\mathbf{U}_l$, $\mathbf{U}_l^*$	Darcy- and large-scale intrinsic average liquid velocity, respectively, $\mathrm{m\,s^{-1}}$
$\mathcal{V}$, $\mathcal{V}_\infty$	Total volume of REV for the Darcy- and large-scale volume averaging, respectively, $\mathrm{m^3}$
$\mathcal{V}_l$, $\mathcal{V}_i$, $\mathcal{V}_s$	Volume of the liquid phase, the insoluble solid and the soluble solid within an REV, $\mathrm{m^3}$
$\mathbf{V}_l$,$\mathbf{V}_l^*$	Darcy- and large-scale superficial average liquid velocity, $\mathrm{m\,s^{-1}}$

Greek letters

α, α^*	Darcy- and large-scale mass exchange coefficient, $\mathrm{s^{-1}}$
α_0, $\alpha_{0,\eta}$, $\alpha_{0,\omega}$	Mass exchange coefficient constant, $\mathrm{s^{-1}}$
$\widehat{\alpha}_0$	Averaged mass exchange coefficient constant within an REV, $\mathrm{s^{-1}}$

$\varepsilon_l, \varepsilon_i, \varepsilon_s$	Volume fraction of the liquid phase, the insoluble solid and the soluble solid, respectively, dimensionless
$\varepsilon_T, \varepsilon_T^*$	Darcy- and large-scale total porosity, respectively, dimensionless
μ_l	Dynamic viscosity, Pa s
ρ_l, ρ_s	Density of the liquid phase and the soluble solid, respectively, $\mathrm{kg\,m^{-3}}$
φ	Volume fraction of each region within a unit cell, dimensionless

1 Introduction

Dissolution of porous media is fundamental in many subsurface processes, such as karst formations (Guo et al. 2016), salt solution mining (Cooper 2002), geological sequestration of CO_2 (Hao et al. 2019) and petroleum engineering (Golfier et al. 2002) to cite a few among many other applications. Natural geological porous formations are hierarchical systems in general, with heterogeneities spanning over different scales and affecting dissolution processes significantly (Hao et al. 2019; Liu et al. 2019). For example, in the circumstances of geological storage of CO_2, the density-driven flow in heterogeneous formations may not always cause significant convective mixing and dissolved CO_2 becomes immobilized in low-permeability zones in layered systems, which reduces the risk of leakage (Agartan et al. 2015). It was also demonstrated that heterogeneity in groundwater velocity and non-aqueous phase liquid (NAPL) distribution plays a very important role in field-scale simulation of NAPL release and dissolution (Christ et al. 2009; Farthing et al. 2012), with the orders of magnitude of field-scale mass transfer coefficients smaller than local mass transfer rates determined in the laboratory (Parker and Park 2004). Such examples are also available in the dissolution of rocks, with heterogeneity in terms of permeability, porosity, mineralogical distribution for instance affecting the dissolution patterns, the optimal injection rate of acid solutions and the breakthrough time, in the context of improved oil recovery through acidizing (Golfier et al. 2002; Kalia and Balakotaiah 2009; Liu et al. 2019; Panga et al. 2005). Therefore, further investigation of dissolution of heterogeneous porous formation is essential for various applications.

It is widely accepted that an accurate way to get deep insight into dissolution processes is to describe them at the pore-scale level, where the chemical–physical interactions take place (Békri et al. 1995; Luo et al. 2012; Soulaine et al. 2017, 2018). In pore-scale modeling, the full physics of dissolution are considered and the governing equations are solved with specific boundary conditions at the fluid–solid interfaces. No assumption is made about the geometric features of the medium, and the movement of the fluid–solid interface is treated explicitly (Luo et al. 2012; Soulaine et al. 2017). Great efforts have been made and various approaches have been proposed to solve dissolution problems at pore-scale, including the arbitrary Lagrangian–Eulerian (ALE) framework (Luo et al. 2012; Starchenko et al. 2016), level set method (Olsson and Kreiss 2005; Olsson et al. 2007), lattice Boltzmann method (LBM) (Chen et al. 2014; Kang et al. 2014), pore network models (PNM) (Varloteaux et al. 2013; Békri et al. 2015) for examples. Based on investigations at the pore-scale, knowledge has been gained for various problems, for instance the scale dependence of reaction kinetics, the influence of pore-scale heterogeneities on the fluid–mineral interaction and the change of permeability and porosity with dissolution process, etc (Hao et al. 2013; Kang et al. 2002, 2014). However, pore-scale modeling is challenging and computationally limited due to several reasons. Firstly, the microscopic information, for instance the spatial distribution of the fluid and the solid, is often difficult

to obtain. Secondly, when considering a large-scale problem at decimetric to metric scales, which is concerned in practical applications, it is impractical and even impossible to take into account of the micrometer-sized pore-scale details. Further difficulties include explicit treatment of the moving interface and handling of non-differentiable surfaces which may be created by the dissolution process, etc (Luo et al. 2012; Vignoles et al. 2010; Soulaine et al. 2018). Therefore, there is a great need to formulate dissolution problems at larger scales.

Darcy-scale (macroscale) models filter pore-scale details and represent them by several macroscale effective parameters, which are obtained by solving corresponding "closure problems" available from the upscaling technique. There is an extensive literature concerning about the upscaling of the transport equations for a given chemical species. The early fundamental works dealt with *passive* dispersion in porous media (Taylor 1953, 1954; Aris 1956) , i.e., advection and diffusion, while they did not consider interaction at the phase interfaces. This problem was later investigated by different upscaling techniques (Brenner and Stewartson 1980; Eidsath et al. 1983; Mei 1992), which led to the classical macroscale dispersion theory and the proposition of local closure problems used to calculate the dispersion tensor components for various representative unit cells. Later, the theory was used in the investigation of *active* dispersion (Quintard and Whitaker 1994a; Bousquet-Melou et al. 2002; Coutelieris et al. 2006; Guo et al. 2015), i.e., transport with interface mass transfer. The resulting Darcy-scale models involves an effective mass exchange term combining the transport to/from the interface with the actual boundary condition at the interface (thermodynamic equilibrium, chemical reaction), as reported in Guo et al. (2015). For the sake of simplicity, the average mass exchange term is often estimated as a first-order expression in terms of difference between the Darcy-scale concentration and the thermodynamic equilibrium concentration, multiplied by a mass exchange coefficient (Quintard and Whitaker 1994a; Coutelieris et al. 2006; Guo et al. 2015; Luo et al. 2014). Two major difficulties have to be overcome in practical applications of such models: (i) dissolution history must be taken into account in the effective parameter correlations and (ii) unstable dissolution patterns may develop such as wormhole formation (Golfier et al. 2002; Panga et al. 2005; Kalia and Balakotaiah 2007; Cohen et al. 2008; Szymczak and Ladd 2011; Liu et al. 2019).

The Darcy-scale model upscaled from the pore-scale equation is valid at a relatively small-scale (millimeter- or centimeter-scale), straightforward use of this Darcy-scale model to larger-scale problems without additional treatments are not appropriate. Indeed, application of Darcy-scale description at real field-scale requires very fine spatial discretization, which is computationally expensive and difficult. Furthermore, physical properties are scale-dependent (Hao et al. 2019). For example, the reaction rate coefficient measured in the field is several orders of magnitude smaller than that obtained at laboratory scale (Hao et al. 2019; White and Brantley 2003; Banwart 1998). Therefore, it is essential to consider further upscaling of the Darcy-scale equations into larger scale, with different types of Darcy-scale heterogeneities taken into consideration. Theoretical development of large-scale models has been investigated by many researchers using various techniques (Bourgeat 1984; Quintard and Whitaker 1987, 1988; Kitanidis 1988; Säez et al. 1989; Dagan 1989; Gelhar et al. 1992; Renard and de Marsily 1997). The method of volume averaging will be adopted in this paper, following previous work published for the upscaling of one-phase and two-phase flows and dispersion in heterogeneous porous media. In an early work (Quintard and Whitaker 1987), the authors dealt with the closure problems for the prediction of large-scale permeability tensor, considering the effect of significant heterogeneities. Later, many investigations of the large-scale mass and momentum transport

equations were carried out for different situations, especially in terms of two-region (or two-medium) models (Chastanet and Wood 2008; Cherblanc et al. 2007, 2003; Golfier et al. 2007; Ahmadi et al. 1998; Tran Ngoc et al. 2020). These works discussed the solutions of various effective parameters appearing in the large-scale model under different assumptions and investigated the impact of different parameters, such as permeability contrasts and volume fraction of each region, on the macroscale effective parameters. More recently, Chabanon et al. (2017) have developed large-scale momentum transport equations for a three-region (porous–porous–solid) medium under local mechanical equilibrium condition and discussed the dependence of effective permeability on several factors. However, very few studies consider mass and momentum transport with dissolution process. Among various investigations, Mabiala et al. (2003) developed a simple large-scale model for NAPL dissolution and provided analytical solutions for the effective parameters. Assuming the large-scale flow is 1D, Golfier et al. (2004) upscaled the Darcy-scale dissolution model into a core-scale two-equation model for local mass equilibrium dissolution and into a one-equation model for local mass non-equilibrium dissolution. Correlations for the effective parameters appearing in the two core-scale models were discussed in Golfier et al. (2006). In addition to such theoretical studies, Hao et al. (2019) used high-resolution simulation to calibrate centimeter-sized models to meter-sized models, with the latter maintaining the same high grid resolutions as the former one, from an empirical perspective.

While various large-scale models have been proposed for specific cases and different kinds of problems, large-scale model for fluid flow coupled with solid/mineral dissolution still remains an open problem. Therefore, we set the objective of this paper as developing a large-scale model for the dissolution of Darcy-scale heterogeneous porous media, without considerations of the mechanical deformations of the heterogeneous porous matrix and their consequences in the change of porosity and the mechanical stability (Laouafa et al. 2011; Prunier et al. 2009, 2009). The rest of the paper is organized as follows. We first apply large-scale volume averaging to the Darcy-scale equations to obtain a large-scale model provided *several constraints* are satisfied. After that, the algorithm to calculate the large-scale effective parameters are presented and the large-scale model developed in this paper is validated by comparing the results with direct numerical simulations, for conditions compatible with the above mentioned constraints and beyond.

2 Development of Large-Scale Dissolution Models

We consider a heterogeneous system as schematically illustrated in Fig. 1, which is composed of two types of rocks, ω and η. Fluid flow creates a dissolution front with a characteristic length scale denoted as ℓ_d, i.e., the zone where the dissolution process is active and materialized by variations of the rock properties, for instance porosity, permeability tensor and so on. The magnitude of ℓ_d has different possibilities in comparison with other characteristic lengths, which will be discussed later. It is assumed that all porous rocks have some insoluble materials, so porosity is always lower than unity (i.e., there is no pure macroscale fluid domain developing during dissolution). The pore-scale characteristic lengths are denoted as ℓ_α, where $\alpha = l$, i and s for the liquid phase flowing into the pore space, the insoluble material and the soluble material, respectively. The Darcy- and large-scale characteristic lengths are denoted as ℓ_ω and ℓ_η, and L, respectively, as illustrated in Fig. 1. We use $\mathcal{V}$ to denote the total volume of the representative elementary volume (REV) used to define the Darcy-scale variables, and $\mathcal{V}_l$, $\mathcal{V}_s$ and $\mathcal{V}_i$ are employed to represent the volumes of

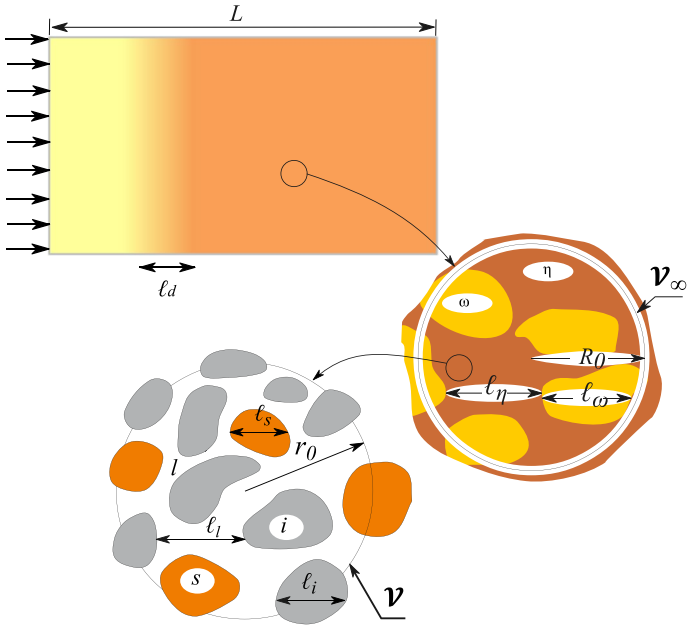

Fig. 1 Schematic illustration of the multi-scale features of a heterogeneous porous formation in the dissolution context

the liquid phase, the soluble and the insoluble solids within the REV, respectively. Assuming that the domain is saturated with liquid, we have $\mathcal{V} = \mathcal{V}_l + \mathcal{V}_s + \mathcal{V}_i$. The actual medium porosity and the volume fractions of the soluble and insoluble solids are defined as

$$\varepsilon_l = \frac{\mathcal{V}_l}{\mathcal{V}}; \; \varepsilon_s = \frac{\mathcal{V}_s}{\mathcal{V}} \text{ and } \varepsilon_i = \frac{\mathcal{V}_i}{\mathcal{V}} \tag{1}$$

respectively. These definitions give

$$\varepsilon_l + \varepsilon_s + \varepsilon_i = 1 \tag{2}$$

With the ongoing of dissolution process, ε_l may evolve from its initial value to the maximum value ε_T, where ε_T is the maximum or total porosity and it is equal to $1 - \varepsilon_i$. It is convenient to define a soluble solid saturation as

$$S = \varepsilon_s / \varepsilon_T \tag{3}$$

which should be distinguished from the normalized concentration of the dissolved material with respect to its thermodynamic equilibrium value. Without entering into the classical discussion of the existence of REV or not, we assume an initial separation of the formation characteristic scales, i.e.,

$$\ell_\alpha \ll \ell_\omega, \ell_\eta \ll L \tag{4}$$

Considering the hierarchical structure schematically illustrated in Fig. 1, a first upscaling can be applied to the pore-scale model to obtain a Darcy-scale model based on the separation of scale assumption expressed by

$$\ell_\alpha \ll r_0 \ll \ell_\omega, \ell_\eta \tag{5}$$

where r_0 is the characteristic size of the Darcy-scale REV as defined in Fig. 1. If constraint given by Eq. 5 is completed with the addition constraint $\ell_d \gg r_0$ (the comparison between ℓ_d and ℓ_ω, ℓ_η will be discussed later in this paper), upscaling can be achieved in the context of reactive porous media, for instance, by using the method of volume averaging (Quintard and Whitaker 1999; Whitaker 1999; Golfier et al. 2002; Coutelieris et al. 2006; Guo et al. 2016). Only this first upscaling incorporates the boundary conditions at the various pore-scale interfaces into the averaged equations and all successive large-scale averaging procedures simply incorporate the influence of heterogeneities into the averaged equations. Whether the Darcy-scale models can be upscaled depends on a further analysis of the separation of scale constraints, i.e., it requires to compare ℓ_d with the other large-scale characteristic lengths of the problem.

- If we have

$$\ell_d \ll \ell_\omega, \ell_\eta \ll L \tag{6}$$

then sharp fronts develop and it is generally difficult to envisage an homogenized model in the large-scale REV (denoted as R_0) of the heterogeneous medium, even if the separation of scales holds for the *initial* description of the heterogeneous system, i.e.,

$$\ell_\omega, \ell_\eta \ll R_0 \ll L \tag{7}$$

- In the condition where

$$\ell_\omega, \ell_\eta \sim \ell_d \ll L \tag{8}$$

it is also necessary to model the problem at the Darcy-scale with an explicit representation of the heterogeneity.

- Finally, one may in principle obtain a homogenizable situation for large-scale upscaling if

$$\ell_\omega, \ell_\eta \ll \ell_d \ll L \tag{9}$$

In such case, spatial variations of porosity induced by dissolution in each Darcy-scale domain, ω and η, will stay small. Hence, the properties of each heterogeneous region are also approximately spatially uniform, even though they indeed evolve with time, and this is a good situation for developing a large-scale model, i.e., a model with effective properties incorporating the effect of the Darcy-scale heterogeneities and dissolution. The separation of scale assumption would read

$$\ell_\alpha \ll r_0 \ll \ell_\omega, \ell_\eta \ll R_0 \ll \ell_d \ll L \tag{10}$$

Since dissolution will change the pore-scale size and structure, the associated local permeability will change, and therefore, the momentum equation must also be upscaled in conjunction with solute transport.

2.1 Darcy-Scale Model

Dissolution of interfaces involve many different thermodynamic and chemical reaction processes. The Darcy-scale model used in this paper is developed from a pore-scale model with nonlinear reactions, which also covers the thermodynamic equilibrium condition, using the method of volume averaging (Whitaker 1999). Such an upscaling from pore-scale to Darcy-scale has been extensively discussed in the literature and we refer the reader to related works (Guo et al. 2016, 2015; Whitaker 1999) for more information. What are the Dary- to large-scale upscaling technical difficulties? The fundamental problems are because Darcy-scale dissolution properties which change with time and exchange terms, in particular exchange coefficients, are heterogeneous. Of course, there might be additional features which will pose certainly tremendous difficulties in terms of upscaling: multi-component aspects, other couplings. In this paper, we adopt one of the simplest problems that covers the two fundamental aspects described above. The Darcy-scale local non-equilibrium mass balance equations can be summarized as:

$$\frac{\partial \rho_s \varepsilon_s}{\partial t} = K_s \tag{11}$$

for the solid phase,

$$\frac{\partial \rho_l \varepsilon_l}{\partial t} + \nabla \cdot \left(\rho_l \mathbf{V}_l\right) = -K_s \tag{12}$$

for the liquid phase and

$$\frac{\partial C_l \varepsilon_l}{\partial t} + \nabla \cdot \left(C_l \mathbf{V}_l\right) = \nabla \cdot \left(\varepsilon_l \mathbf{D}_l \cdot \nabla C_l\right) - K_s \tag{13}$$

for the dissolved mineral, where ρ_s and ρ_l denote the densities of the dissolved mineral and the liquid phase, respectively, K_s denotes the mass exchange term of the dissolved mineral, $\mathbf{V}_l$ denotes the Darcy-scale superficial average velocity, C_l denotes the Darcy-scale intrinsic average mass concentration of the dissolved mineral, $\mathbf{D}_l$ denotes the active dispersion tensor. Even though K_s is in fact dependent on higher orders of concentration difference $\left(C_l - c_{eq}\right)$, with c_{eq} the thermodynamic equilibrium mass concentration of the dissolved mineral, a first-order estimation was widely adopted in the previous studies (Guo et al. 2016; Cherblanc et al. 2007; Gwo et al. 1996; Gvirtzman et al. 1988) because the accuracy is sufficient for many practical situations when considering the large number of uncertainties (Cherblanc et al. 2007). In this paper, we also take

$$K_s = \alpha\left(C_l - c_{eq}\right) \tag{14}$$

for the sake of simplicity and accurate expressions of the mass exchange term obtained by solving pore-scale closure problems with different boundary conditions were discussed in a previous work (Guo et al. 2015). Here, α is called the mass exchange coefficient, which is concentration-dependent and generally expressed as a constant, α_0, times a function of the solid saturation (eventually a dependency upon some other microscale dimensionless parameters such as Péclet number and Reynolds number), i.e.,

$$\alpha = \alpha_0 \, \alpha'(S) \tag{15}$$

From Eqs. 11 and 12, we have

$$\nabla \cdot \mathbf{V}_l = -K_s \left(\frac{1}{\rho_l} - \frac{1}{\rho_s} \right) \tag{16}$$

with the assumption of constant liquid density. The filtration velocity within each region must also be described by a macroscale equation. Starting with the pore-scale Navier–Stokes equations, assuming that the Reynolds number is small enough and dissolution slow enough in comparison with viscous relaxation, it can be shown that the macroscale momentum balance equation has the form of a Darcy's law (Whitaker 1986)

$$\mathbf{V}_l = -\frac{\mathbf{K}_l}{\mu_l} \cdot \left(\nabla P_l - \rho_l \mathbf{g} \right) \tag{17}$$

where $\mathbf{K}_l$ is the permeability tensor depending on the position (i.e., the rock type at the given position), P_l denotes Darcy-scale intrinsic average pressure and $\mathbf{g}$ denotes gravitational acceleration. Since dissolution will change the pore-scale structure, it is clear that $\mathbf{K}_l$ depends on the dissolution history (Békri et al. 1995; Golfier et al. 2006; Luquot and Gouze 2009). In this paper, we adopt the assumption classically made in geochemistry that the historical dependence of the permeability with dissolution can be approximated through a direct dependence of permeability with the pore volume fraction, i.e., dependence with saturation in our problem.

Two important dimensionless numbers, namely the Darcy-scale Damköhler number (Da_M), which tells whether the macroscale flow is controlled by the mass exchange or diffusion at the reference scale ℓ_h and the Darcy-scale Péclet number (Pe_M), which shows the competition of mass transport between convection and diffusion, are defined by

$$\mathrm{Da}_M = \frac{\alpha_0 \ell_h^2}{D_r} \tag{18}$$

and

$$\mathrm{Pe}_M = \frac{U_r \ell_h}{D_r} \tag{19}$$

respectively. Here, U_r and D_r represent the reference velocity and reference diffusion coefficient, respectively. ℓ_h is taken as the characteristic length of the heterogeneities for heterogeneous formations with repeated pattern or L for a problem which is not susceptible of an intermediate upscaling (i.e., continuously varying heterogeneities, with correlation lengths up to L).

Various issues encountered in large-scale averaging, in particular the question of scale separation, are discussed in Supplementary Information. As a conclusion of the discussion, we summarize the assumptions made to implement large-scale averaging as following:

- Fluid density and viscosity are locally constant. For the most widespread soluble rocks in nature, the density variation of saturated solution of carbonate rocks or gypsum compared to freshwater are smaller than 3%. Larger density variation may take place for the dissolution of halite (NaCl); however, because the solution is far from saturation (rock solubility) in the uniform dissolution regime, the component of the liquid phase will not change too much; therefore, it is reasonable to assume that the fluid density and viscosity are unchanged within an REV.

- Fluid flow is at low Reynolds number such that inertia terms may be neglected in the upscaling problem,
- Dissolution is described by the local non-equilibrium case,
- Mass exchange coefficient depends only on saturation,
- Dissolution rate is slow, so the total mass balance equation may be approximated by $\nabla \cdot \left(\varepsilon_T(1-S)\,\mathbf{U}_l\right) = 0$ (a kind of generalized Boussinesq approximation which is acceptable for low-solubility material or cases for which the water density does not change significantly (Abriola and Pinder 1985)),
- Dispersion and diffusion are neglected compared to advection (which corresponds to many situations encountered in hydrology) because the concentration deviation is close to zero, which will be explained in detail later.

These assumptions enable us to simplify the Darcy-scale model introduced above into the following form

$$\nabla \cdot \left(\varepsilon_T(1-S)\,\mathbf{U}_l\right) = 0 \tag{20a}$$

$$\varepsilon_T(1-S)\frac{\partial C_l}{\partial t} + \varepsilon_T(1-S)\,\mathbf{U}_l \cdot \nabla C_l = -\alpha\left(C_l - c_{eq}\right) \tag{20b}$$

$$\varepsilon_T \frac{\partial S}{\partial t} = \frac{1}{\rho_s}\alpha\left(C_l - c_{eq}\right) \tag{20c}$$

$$\mathbf{V}_l = \varepsilon_T(1-S)\,\mathbf{U}_l = -\frac{1}{\mu_l}\mathbf{K}_l \cdot \left(\nabla P_l - \rho_l \mathbf{g}\right) \tag{20d}$$

Here, effective properties such as ε_T, α, $\mathbf{K}_l$ depend on position to reflect the Darcy-scale heterogeneities. The main unknown variables are the continuous fields C_l and P_l, and the possibly discontinuous field S, for which the governing equation has no fluxes. Normal fluxes are also continuous through inter-region boundaries; therefore, heterogeneities (and inter-region interfaces) are dealt with in the sense of distributions (Marle 1982; Gray et al. 1993; Quintard and Whitaker 1994b).

2.2 Large-Scale Volume Averaging

Large-scale volume averaging can be developed with a general averaging scheme involving a convolution product (Quintard and Whitaker 1994b; Davit and Quintard 2017). For the sake of simplicity, we simply use in the notations a basic kernel that leads to large-scale averages defined as

$$\left\{\varepsilon_T\right\} = \frac{1}{\mathcal{V}_\infty}\int_{\mathcal{V}_\infty} \varepsilon_T\, dV \tag{21}$$

for the averaged total porosity, with braces used to denote large-scale averages instead of the brackets used for Darcy-scale averages. The large-scale saturation, S^*, can be defined as

$$\left\{\varepsilon_T S\right\} = \left\{\varepsilon_T\right\} S^* \tag{22}$$

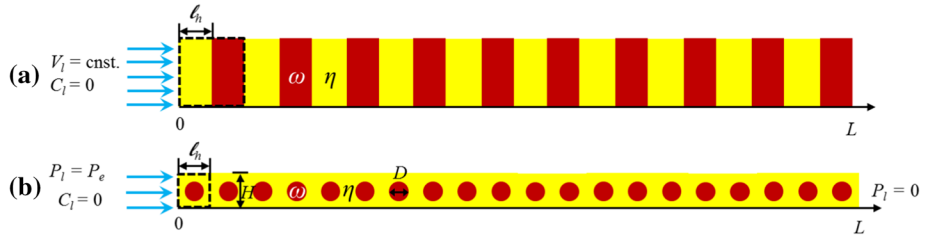

Fig. 2 Schematic illustration of the stratified system (**a**) and the nodular system (**b**), with $\ell_h = H = 0.05$ m and $D = 0.03$ m. Dashed rectangles are used to indicate unit cells

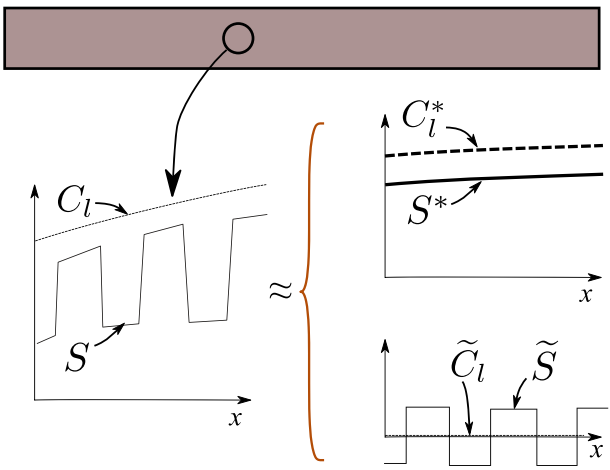

Fig. 3 Sketch of the multiple-scale dissolution problem and the REV-scale approximations

and this can be used to define the large-scale concentration, C_l^*, and intrinsic velocity, $\mathbf{U}_l^*$, as

$$\left\{\varepsilon_T(1-S)\,C_l\right\} = \left\{\varepsilon_T\right\}(1-S^*)\,C_l^* \tag{23}$$

$$\left\{\varepsilon_T(1-S)\,\mathbf{U}_l\right\} = \left\{\varepsilon_T\right\}(1-S^*)\,\mathbf{U}_l^* \tag{24}$$

The spatial deviations for concentration and saturation are defined as

$$C_l = C_l^* + \tilde{C}_l \tag{25}$$

$$S = S^* + \tilde{S} \tag{26}$$

Note that $\tilde{C}_l$ and $\tilde{S}$ have completely different behaviors. Taking the stratified system shown in Fig. 2a for example, since the stratified domain is initially saturated with the dissolved mineral at thermodynamic equilibrium concentration while solid saturation S is dependent on rock type (as discussed in Supplementary Information), the concentration deviation is zero for a uniform C_l-field and $\tilde{S}$ has initially the crenelated shape, as represented in Fig. 3.

Through the derivation as provided in Supplementary Information, we obtained the coupled Darcy-scale/large-scale problem for the case of small Damköhler numbers, which can be approximated by the following equations

$$\frac{\partial}{\partial t}\left(\left\{\varepsilon_T\right\}(1-S^*)\,C_l^*\right)+\nabla\cdot\left(\left\{\varepsilon_T\right\}(1-S^*)\,\mathbf{U}_l^*\,C_l^*\right)=-\alpha^*\left(C_l^*-c_{eq}\right) \tag{27a}$$

$$\frac{\partial}{\partial t}\left(\left\{\varepsilon_T\right\}S^*\right)=\frac{1}{\rho_s}\alpha^*\left(C_l^*-c_{eq}\right) \tag{27b}$$

$$\varepsilon_T\frac{\partial}{\partial t}\tilde{S}=\frac{1}{\rho_s}\left(\alpha-\frac{\varepsilon_T\alpha^*}{\left\{\varepsilon_T\right\}}\right)\left(C_l^*-c_{eq}\right) \tag{27c}$$

where $\alpha^*=\{\alpha(S)\}$ is not expressed yet under a closed form, i.e., in terms of averaged variables. When considering the case of constant mass exchange coefficient in each region within the REV, α^* is perfectly defined as $\alpha^*=\{\alpha\}$ and the averaged equations have a completely closed form, i.e., involving large-scale averaged values only. In most cases, however, α is not constant and depends primarily upon the local value of S in a nonlinear way as well as on the rock type. Since the time evolution of $\tilde{S}$ features *history/memory effects*, the properties to be homogenized are not only space-dependent but also time-dependent through a dissolution history function of the considered process.

2.2.1 Approximate Mass Balance Equations

Here we propose to estimate $\tilde{S}$ and hence the mass exchange coefficient and other transport properties for the case of small Damköhler numbers in an approximate manner using Eqs. 27b and 27c. Combining these equations, we obtain

$$\varepsilon_T\,\frac{\partial\tilde{S}}{\partial t}=\left(\left\{\varepsilon_T\right\}\alpha-\varepsilon_T\alpha^*\right)\frac{1}{\alpha^*}\,\frac{\partial S^*}{\partial t} \tag{28}$$

or

$$\frac{\partial S}{\partial t}=\frac{\left\{\varepsilon_T\right\}\alpha}{\varepsilon_T\alpha^*}\,\frac{\partial S^*}{\partial t} \tag{29}$$

which can be used to build, *assuming an arbitrary evolution of the large-scale saturation*, a large-scale correlation for α^*.

An explicit first-order approximation of this ordinary differential equation would read

$$S_{n+1}=S_n+\left(\frac{\left\{\varepsilon_T\right\}\alpha(S_n)}{\varepsilon_T\alpha^*(S_n^*)}\right)_n\left(S_{n+1}^*-S_n^*\right) \tag{30}$$

where n and $n+1$ refer to dissolution stages. It is important to notice that time does not explicitly appear in this equation. Since S_{n+1} depends only on the saturation fields and a given evolution of the large-scale saturation in the previous step, this feature can be used to build $\alpha^*(S^*)$ through the following sequence:

1. Assume the initial saturation in the medium S_0 is known, which also determines S_0^*.

2. Assume a given large-scale saturation dissolution increment, δS^*: then $S^*_{n+1} = S^*_n - \delta S^*$ (since S_0 is the maximum value, the sequence is a decreasing sequence)
3. Compute S_{n+1} using Eq. 30, Note at this point that, *whatever the evolution history of* S^*, there is a direct relation between S and S^*. This was made possible by the assumption that concentration deviation was negligible within the REV, an assumption itself linked to the small value of the Damköhler numbers.
4. As a consequence, all Darcy-scale properties are determined, in particular $\alpha(S_{n+1})$ and $K_l(S_{n+1})$
5. Compute $\alpha^*(S^*_{n+1}) = \{\alpha(S_{n+1})\}$
6. Compute $\mathbf{K}^*_l(S^*_{n+1})$, if necessary
7. Iterate until large-scale saturation is zero.

The large-scale equations describing the mass balances would read:

$$\nabla \cdot \left(\{\varepsilon_T\}(1 - S^*)\, \mathbf{U}^*_l \right) = 0 \tag{31a}$$

$$\frac{\partial}{\partial t}\left(\{\varepsilon_T\}(1 - S^*)\, C^*_l \right) + \nabla \cdot \left(\{\varepsilon_T\}(1 - S^*)\, \mathbf{U}^*_l\, C^*_l \right) = -\alpha^*(S^*) \left(C^*_l - c_{eq} \right) \tag{31b}$$

$$\frac{\partial}{\partial t}\left(\{\varepsilon_T\}\, S^* \right) = \frac{1}{\rho_s} \alpha^*(S^*) \left(C^*_l - c_{eq} \right) \tag{31c}$$

2.2.2 Upscaling Darcy's Law

From the algorithm outlined above, S^* is bijectively associated with Darcy-scale values of S at each dissolution step. As a consequence, the Darcy-scale values of the relative permeability are also specified. Therefore, we only need to average, for each value of S^*, a problem corresponding to

$$\nabla \cdot \mathbf{V}_l = 0 \tag{32a}$$

$$\mathbf{V}_l = -\frac{\mathbf{K}_l(S)}{\mu} \cdot \left(\nabla P_l - \rho_l \mathbf{g} \right) \tag{32b}$$

This is the classical problem of upscaling heterogeneous permeability fields, and there is an intense literature on the subject (Sánchez-Vila et al. 1995; Renard and de Marsily 1997). From upscaling techniques point of view, this problem has already been treated and leads to a large-scale Darcy's law of the form (see for instance Refs. (Bourgeat 1984; Quintard and Whitaker 1987, 1988; Säez et al. 1989))

$$\mathbf{V}^*_l = \{\mathbf{V}_l\} = \{\varepsilon_T\}(1 - S^*)\, \mathbf{U}^*_l = -\frac{\mathbf{K}^*_l(S^*)}{\mu_l} \cdot \left(\nabla P^*_l - \rho_l \mathbf{g} \right) \tag{33}$$

where $\mathbf{K}^*_l(S^*)$ is the large-scale permeability at the given large-scale saturation and P^*_l is the large-scale intrinsic average pressure. Following the cited literature, this effective permeability is computed by solving an intermediate local problem for a mapping vector $\mathbf{b}$ such that

$$P_l = P_l^* + \mathbf{b} \cdot \left(\nabla P_l^* - \rho_l \mathbf{g} \right) \tag{34}$$

For periodic unit cells, $\mathbf{b}$ is a continuous field determined by the following closure problem:

$$\nabla \cdot \left(\mathbf{K}_l \cdot \nabla \mathbf{b} + \mathbf{K}_l \right) = 0 \tag{35a}$$

$$\{\mathbf{b}\} = 0 \tag{35b}$$

$$\mathbf{b}\left(\mathbf{r} + \ell_i\right) = \mathbf{b}(\mathbf{r}) \tag{35c}$$

For non-periodic unit cells, Eq. 35c cannot be used, and one reverts to various types of problems and boundary conditions, like permeameter conditions as discussed in Renard and de Marsily (1997), Guibert et al. (2016). A large variety of estimates and bounds are also available in Renard and de Marsily (1997).

To conclude, a large-scale modeling would involve, firstly, solving the various closure problems to provide tables for $\alpha^*(S^*)$ and $\mathbf{K}_l^*(S^*)$ and, secondly, solving the specific large-scale initial boundary value problem described by Eqs. 31 and 33, with appropriate initial and boundary conditions, using the large-scale properties computed at step #1 above.

3 Validation of Large-Scale Models

We have shown how to develop a fully homogenized large-scale model including history effect, and this involved the important assumption that the diffusive and convective Damköhler numbers must be small enough. In this section, we test the proposed approach by considering two organized systems as shown in Fig. 2, with one being a stratified system and the other being a 2D nodular system. For the computations of these two systems, without losing generality, we use pure gypsum dissolution in water as an example while it could also be halite and carbonates, etc. The parameters used are presented in Table 1 and the computations were performed with the finite element software COMSOL Multiphysics®. In the large-scale model, the effective total porosity and effective initial soluble solid saturation are obtained by

$$\varepsilon_T^* = \varphi_\eta \varepsilon_{T,\eta} + \varphi_\omega \varepsilon_{T,\omega} \tag{36}$$

Table 1 Properties of the liquid, the solid and the porous media

Parameter	Value
ρ_l	$1000\ \mathrm{kg\,m^{-3}}$
ρ_s	$2310\ \mathrm{kg\,m^{-3}}$
D_r	$10^{-9}\ \mathrm{m^2\,s^{-1}}$
c_{eq}	$2.5\ \mathrm{kg\,m^{-3}}$
ε_T	0.35 in η region, 0.25 in ω region
$S(t=0)$	0.1 in η region, 0.15 in ω region
K_0	$10^{-11}\ \mathrm{m^2}$ in η region, $10^{-12}\ \mathrm{m^2}$ in ω region
K_l	$K_0(1-S)^3$ in η region, $K(1-S)^2$ in ω region

$$S^* = \left(\varphi_\eta \varepsilon_{T,\eta} S_\eta + \varphi_\omega \varepsilon_{T,\omega} S_\omega\right) / \varepsilon_T^* \tag{37}$$

where φ_η, $\varepsilon_{T,\eta}$ and S_η represent the volume fraction of ηregion within a unit cell, the total porosity and the initial solid saturation in η region, respectively. Their counterparts in ω region are denoted as φ_ω, $\varepsilon_{T,\omega}$ and S_ω, respectively.

For both the stratified and the nodular systems, initially they have thermodynamic equilibrium concentration of the dissolved mineral. Then freshwater with zero concentration of the dissolving mineral flows into the system from the left boundary and flows out at the right boundary. For the stratified system, the filtration velocity is imposed as Dirichlet boundary condition. As a consequence, the filtration velocity $\mathbf{V}_l^*$ for this 1D problem is constant and equals to the entrance filtration velocity. Therefore, there is no need to work out the problem of the momentum equation and we only need to solve the coupled equations 20b, c for the Darcy-scale model and 31b, c for the large-scale model. Thus, the only unknown effective parameter is $\alpha^*(S^*)$. To illustrate a more complex situation for the nodular system, Dirichlet conditions were imposed for the Darcy-scale pressure at the inlet ($P_l = P_e$) and outlet ($P_l = 0$) boundaries. As dissolution occurs, the variation of the local permeability will generate a change in the Darcy-scale and large-scale filtration velocities which must be calculated when solving the large-scale problem. Therefore, $\mathbf{K}_l^*(S^*)$ has also to be determined as explained in Sect. 2.2. In addition to mass balance equations, momentum Eqs. 20d and 33 are also essential to be solved for the Darcy- and large-scale models, respectively. When solving large-scale Darcy's law in the numerical simulations, the following boundary conditions were adopted: $P_l^* = P_e$ at the inlet and $P_l^* = 0$ at the outlet. Taking the same Dirichlet conditions for the two scales leads to a small error on the order of $\mathcal{O}\left(\frac{\ell_h P_e}{L}\right)$ when comparing the Darcy-scale and large-scale pressure fields. This error decreases with the number of unit cells in the large-scale simulation.

3.1 Calculation of the Large-Scale Effective Parameters

As schematically depicted in Fig. 3, saturation S and concentration C_l are both varying slowly and can be estimated approximately as constants within an REV in the case of small Da_M (constant by rock type for saturation). Since there is a correlation between Darcy-scale mass exchange coefficient α and local saturation S, α can also be considered as a constant in each heterogeneous region η and ω, respectively, *at a given point in the dissolution history*. We obtain effective parameters in the large-scale model by solving closure problems for the deviation of local saturation $\tilde{S}$, i.e., Eq. 30, which can be used to build $\alpha^*(S^*)$ and $\mathbf{K}_l^*(S^*)$ through the sequence provided in the last section. A python code has been developed to solve for the closure problems and compute $\alpha^*(S^*)$ and $\mathbf{K}_l^*(S^*)$, the algorithm of which is schematically illustrated in Fig. 4 for the REV presented therein. More specifically, the effective solid saturation S^* is in a decreasing trend from its initial value with dissolution going on (as indicated by the black arrow in the top figure of Fig. 4). Using Eq. 30, a correlation is obtained between S^* and the corresponding values of S in η and ω regions, respectively. Consequently, Darcy-scale parameters $\alpha(S)$ and $K_l(S)$ can be obtained since they are functions of S. Finally, large-scale parameters $\alpha^*(S^*)$ and $\mathbf{K}_l^*(S^*)$ are obtained by solving "closure problems" as explained in Subsection 2.2.

We performed computations with different values of $\alpha_{0,\eta}$ and consequently different $\alpha_{0,\omega}$ and obtained, respectively, the correlations of the large-scale effective mass exchange coefficient $\alpha^*(S^*)$ and the large-scale permeability $K_l^*(S^*)$ with large-scale soluble solid saturation S^*. The results of $\alpha^*(S^*)/\widehat{\alpha}_0$ as a function of S^* are presented in Fig. 5a, where we

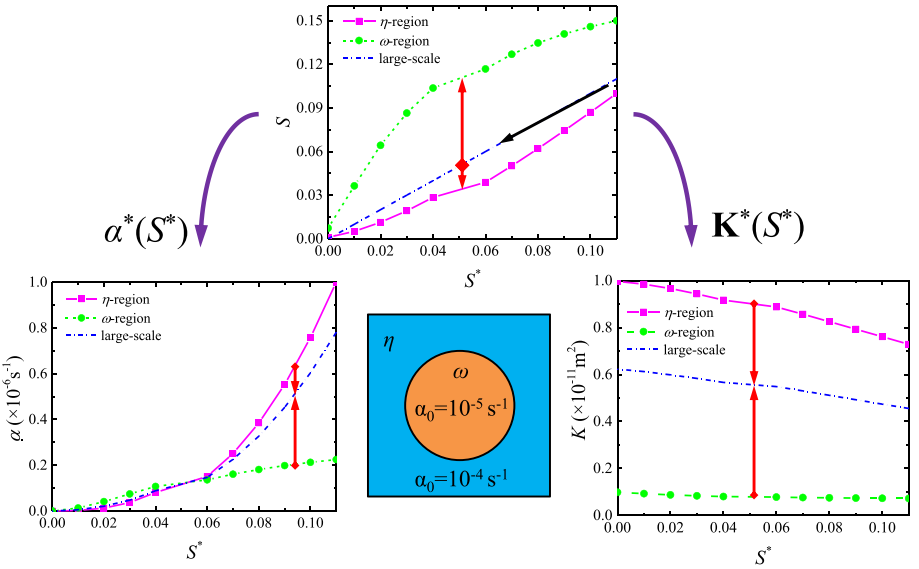

Fig. 4 Illustration of the algorithm for the a priori calculation of large-scale effective properties for the corresponding REV

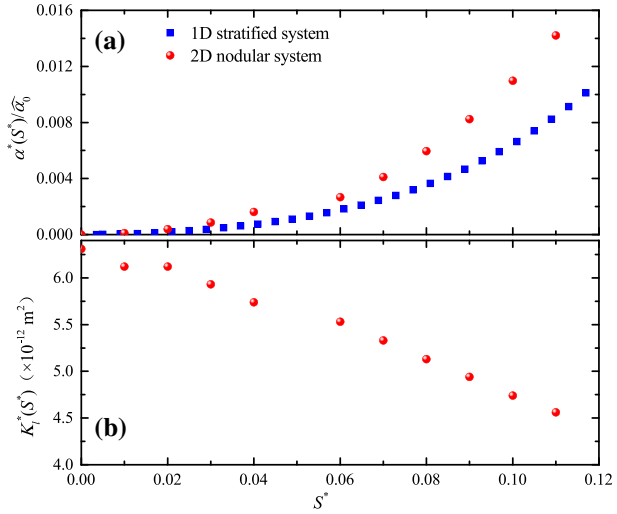

Fig. 5 Normalized large-scale mass exchange coefficient (**a**) and effective permeability (**b**) as a function of large-scale solid saturation

have $\widehat{\alpha}_0 = \varphi_\eta \alpha_{0,\eta} + \varphi_\omega \alpha_{0,\omega}$ with $\alpha_{0,\eta}$ and $\alpha_{0,\omega}$ denoting α_0 in $\eta-$ and $\omega-$region, respectively. We indeed observe the decrease in $\alpha^*(S^*)/\widehat{\alpha}_0$ with the decrease in the solid saturation as expected. In addition, because of the symmetry of the unit cells and the isotropy of the Darcy-scale permeability, the closure problem gives a spherical $\mathbf{K}_l^*$ with $\mathbf{K}_l^*(S^*) = K_l^*(S^*)\mathbf{I}$. The values of $K_l^*(S^*)$ are plotted in Fig. 5b. With the ongoing of dissolution process, porosity is increased with the decrease in the solid saturation, and this leads to larger permeability. The correlations shown in Fig. 5 will be employed later in the large-scale computations.

3.2 Comparison Between Large- and Darcy-Scale Models

After getting solutions for large-scale effective parameters $\alpha^*(S^*)$ and $K_l^*(S^*)$, we carry out large-scale numerical simulations for the two systems mentioned above. The ranges for the characteristic velocity (U_r), the corresponding Darcy-scale Péclet number (Pe_M) and Damköhler number (Da_M and $\mathrm{Da}_M/\mathrm{Pe}_M$) are presented in Table 2, with U_r the infiltration velocity in the 1D case and the average velocity in the 2D case. Three values of Pe_M are used for each system to illustrate the behaviors of the large-scale models in different conditions. The influence of large-scale mass exchange coefficient is investigated in terms of various Da_M and $\mathrm{Da}_M/\mathrm{Pe}_M$. Figure S2 in Supplementary Information shows that the thickness of the dissolution front depends on the value of Da_M at low Pe_M numbers and the value of $\mathrm{Da}_M/\mathrm{Pe}_M$ at high Pe_M numbers. However, for the 2D nodular system, it is difficult to plot a similar diagram like Fig. S2 for the stratified system, because it is hard to have a fully dissolved REV even with sharp dissolving interface, which will be explained later.

3.2.1 Stratified System

For the stratified system, the comparison of saturation between Darcy- (DNS) and large-scale (LS) results with $\mathrm{Pe}_M = 0.5$, 5 and 50 is presented in Fig. 6. The comparison of the normalized concentration of the dissolved solid between Darcy- and large-scale results are plotted in Fig. 7. An overall comment is that the results obtained from Darcy- and large-scale models agree very well with each other. We have shown in Fig. S2 in Supplementary Information that the ordering of the various scales (in particular the front thickness ℓ_d versus ℓ_ω and ℓ_η) depends on Da_M and $\mathrm{Da}_M/\mathrm{Pe}_M$. The good agreement of the results even at high Damköhler numbers with sharp dissolution front (e.g., Fig. 6c, d and h) shows the robustness of the large-scale model developed in this paper. Specifically, one may find that when Pe_M is fixed, increasing Da_M leads to the sharpening of the dissolution front (see each column of Fig. 6), while when Da_M is the same, increasing Pe_M leads to more diffusive dissolution front (see each row of Fig. 6). These phenomena are determined by the competition between mass transport and mass exchange rate.

When the characteristic time of mass transport is smaller than that of mass exchange, the injected liquid is penetrating deep into the porous medium, with a thick dissolution front and vice versa. Comparing Figs. 7a–c, one may find that the thickness of the dissolution front in terms of concentration distribution is highly dependent on $\mathrm{Da}_M/\mathrm{Pe}_M$. The decrease in the dissolution front thickness with increasing $\mathrm{Da}_M/\mathrm{Pe}_M$ is much more profound when $\mathrm{Da}_M/\mathrm{Pe}_M < 2750$, before sharp dissolution front forms at $\mathrm{Da}_M/\mathrm{Pe}_M = 2750$. Then, further increase in $\mathrm{Da}_M/\mathrm{Pe}_M$ only leads to negligible variation of dissolution front thickness because the dissolution process is limited by mass transport. The comparisons in different graphs of Figs. 6 and 7 also show that for a certain $\mathrm{Da}_M/\mathrm{Pe}_M$, the dissolution rate

Table 2 Parameters used for the two systems

Parameter	Stratified system			Nodular system		
U_r (m/s)	10^{-8}	10^{-7}	10^{-6}	3.67×10^{-9}	3.67×10^{-8}	1.85×10^{-7}
Pe_M	0.5	5	50	0.2	2	10
Da_M	138-137500	138-137500	138-137500	1-688	14-688	14-688
$\mathrm{Da}_M/\mathrm{Pe}_M$	275-275000	28-27500	3-2750	7-3437	7-344	1-69

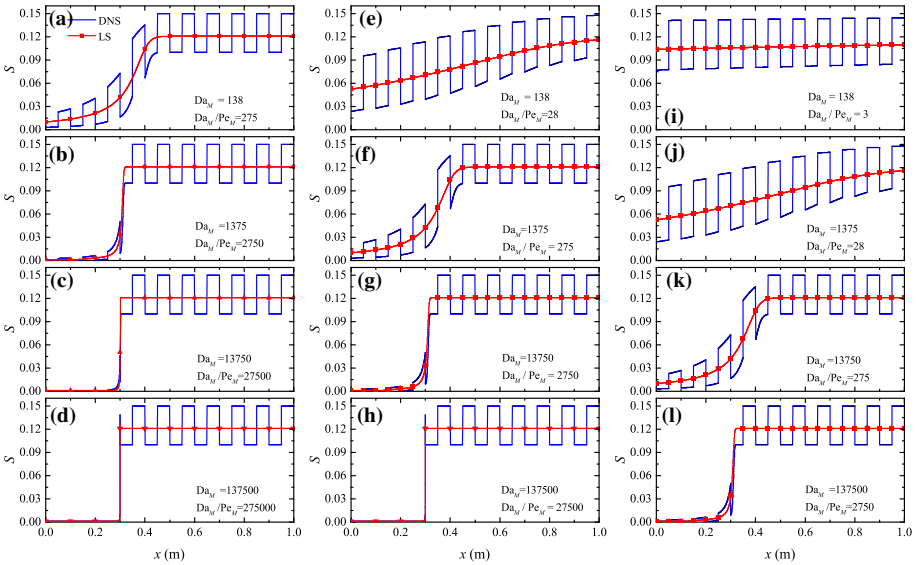

Fig. 6 Comparison of S between Darcy- and large-scale results for various Da_M and $\mathrm{Da}_M/\mathrm{Pe}_M$, respectively. (**a**–**d**) $\mathrm{Pe}_M = 0.5$, $t = 10^9$ s, (**e**–**h**) $\mathrm{Pe}_M = 5$, $t = 10^8$ s and (**i**–**l**) $\mathrm{Pe}_M = 50$, $t = 10^7$ s

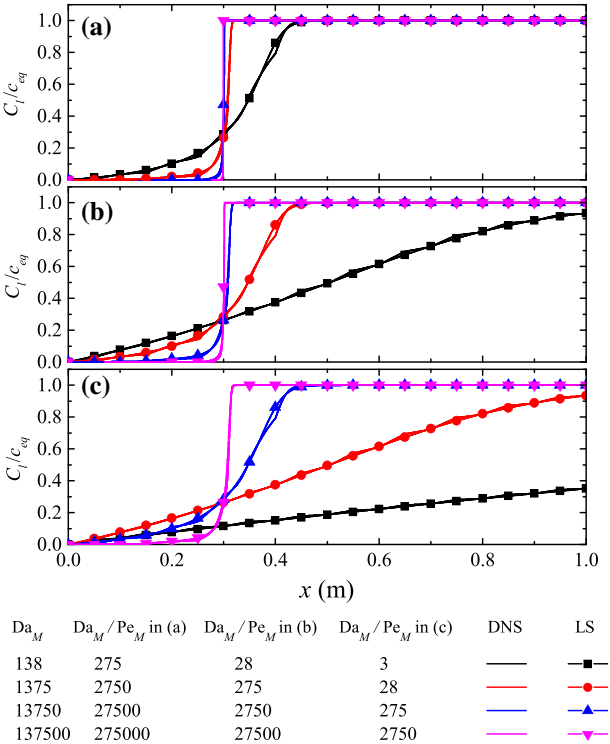

Fig. 7 Comparison of normalized concentration between Darcy- and large-scale results. (**a**) $\mathrm{Pe}_M = 0.5$, $t = 10^9$ s, (**b**) $\mathrm{Pe}_M = 5$, $t = 10^8$ s and (**c**) $\mathrm{Pe}_M = 50$, $t = 10^7$ s

is proportional to Pe_M because increasing Pe_M by one or two orders while decreasing the dissolution time by the same magnitude leads to similar position of the dissolution front (see $\mathrm{Da}_M/\mathrm{Pe}_M = 275$ and 2750 for example).

The robustness of the large-scale model is largely due to topological effects: The flow being one-dimensional, the field characteristic lines are also 1D. The sharp front corresponding to local equilibrium dissolution moves through the REV with a constant direction and no rock type is free from dissolution. As a consequence, the Darcy-scale concentration changes from zero to equilibrium concentration within the REV when crossing the dissolution interface. Therefore, the large-scale average concentration is not equal to the equilibrium concentration and this calls for a large-scale non-equilibrium dissolution model. Interestingly, the proposed theory allows to build such a large-scale non-equilibrium model, even if the theoretical premises are not adequate. Now, if the characteristics develop in a 2D or 3D pattern, regions may be bypassed by the flow and dissolution front. Therefore, the large-scale average concentration will not also be equal to the equilibrium concentration. A large-scale non-equilibrium dissolution model is likely to be a good candidate for reproducing the large-scale averaged behavior, but the building of the history closure problems may be very complicated and rather different from the proposed theory. This will be indeed observed in the case of the nodular system presented below, when the chosen parameters go far beyond the model limitations.

3.2.2 Nodular System

Similar study was carried out for the 2D nodular system and the comparisons between Darcy- and large-scale saturation are presented in Figs. 8a–c for $\mathrm{Pe}_M = 0.2$, 2 and 10, respectively. The results from DNS are averaged values of S in analogy to Eq. 37 within each unit cell as defined in Fig. 2b. Again, we find the good agreement between the Darcy- and large-scale results when the assumption of scale separation is fulfilled, i.e., $\mathrm{Da}_M < 14$ for $\mathrm{Pe}_M = 0.2$ and $\mathrm{Da}_M < 138$ for $\mathrm{Pe}_M = 2$ and 10. When Da_M is larger than these values, there tends to be some discrepancies between Darcy- and large-scale values with large-scale models giving thinner dissolution front. Moreover, this discrepancy is smaller when Pe_M is small, which can be observed in Figs. 8a–c for $\mathrm{Da}_M = 688$. In order to get more details about the saturation field, we plot in Fig. 9 the Darcy-scale saturation distribution corresponding to different cases of Fig. 8a. It is seen that, firstly, the dissolution front is more diffusive when Da_M is small, while the increase in Da_M leads to thinner dissolution front, as already indicated in Fig. 8a. When Da_M is small, the dissolution process is limited by mass exchange and the saturation ratio between the two regions is small; therefore, large-scale models give satisfactory results compared to DNS. However, when Da_M is larger, the dissolution rate is increased much more for the η region (the matrix) than for the ω region (the inclusions), because the former holds a larger initial volume fraction of the liquid phase ($\varepsilon_T(1-S) = 0.315$ for η region versus $\varepsilon_T(1-S) = 0.213$ for ω region) and it is easier for the fluid to flow through η region, which leads to a larger gradient of the concentration difference and consequently faster mass exchange. That is why we see nearly fully dissolved condition in η region while only slightly dissolved condition in ω region in the first couple of unit cells when $\mathrm{Da}_M \geq 69$. Moreover, the obstacle of the upstream inclusions makes the fluid difficult to reach the zones between the neighboring inclusions, where dissolution is insufficient. This effect is more profound when Da_M is larger, while the large-scale model failed to catch this. Therefore, we see in Fig. 8 that, in coherence

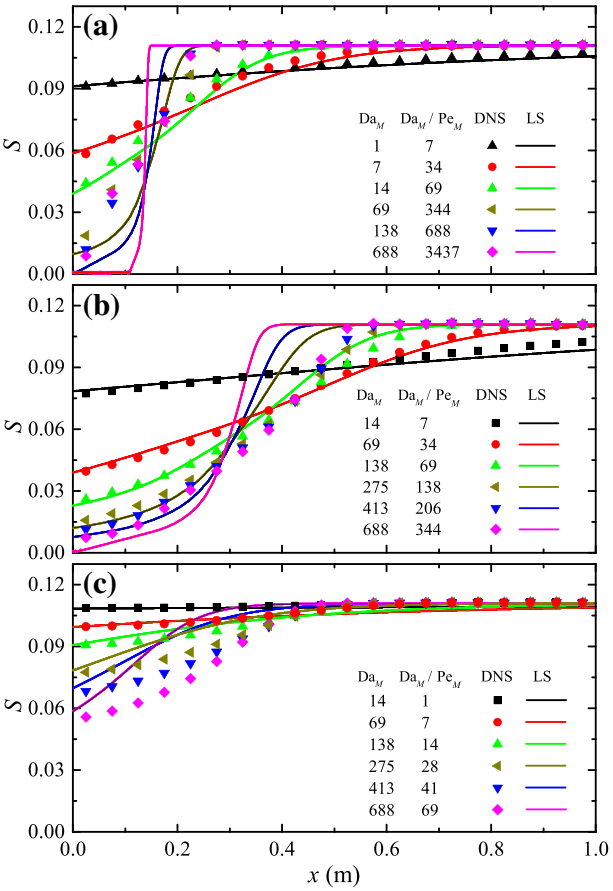

Fig. 8 Comparison of saturation between Darcy- and large-scale results for various Da_M and Da_M/Pe_M, respectively. (**a**) $Pe_M = 0.2$, $t = 10^9$ s, (**b**) $Pe_M = 2$, $t = 2 \times 10^8$ s and (**c**) $Pe_M = 10$, $t = 10^7$ s

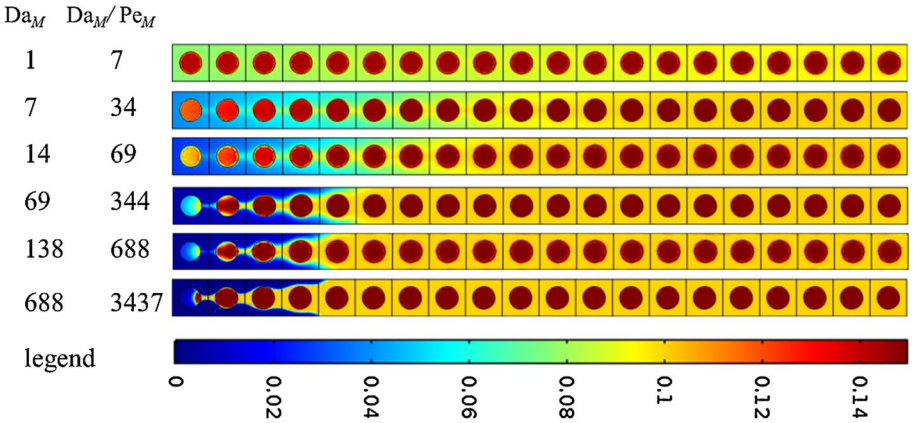

Fig. 9 Darcy-scale saturation distribution corresponding to Fig. 8a, $t = 10^9 s$, $Pe_M = 0.2$

with our discussion on the scale separation problem, the discrepancy between Darcy- and large-scale models grows with increasing Da_M.

As mentioned above, the dissolution front in the large-scale model is thinner than in DNS, which underestimates the saturation on the left half of the dissolving zone while overestimates the saturation on the right half. In order to find out whether the overestimation and underestimation of S by the large-scale model can be compensated, we compared the averaged saturation within the whole domain, and they are denoted as $\widehat{S}$ and $\widehat{S}^*$ in DNS and large-scale model, respectively. The error of the large-scale value is defined as

$$E_S = \frac{\widehat{S}^* - \widehat{S}}{\widehat{S}} \times 100\% \tag{38}$$

and the corresponding results are presented in Fig. 10 for the different cases shown in Fig. 8. It is observed that the relative error for $\mathrm{Da}_M < 200$ are smaller than 3% for all the cases, while when $\mathrm{Da}_M > 200$, the discrepancy remains small for $\mathrm{Pe}_M = 0.2$ but increase dramatically with Da_M for $\mathrm{Pe}_M = 2$ and 10. At $\mathrm{Da}_M = 688$, E_S goes up to about 8% of $\widehat{S}$ for $\mathrm{Pe}_M = 10$. This is again consistent with what we have reported previously that the large-scale model is more suitable for the low Da_M condition, when the variation of parameters within each unit cell is small and smooth, as shown in Fig. 3.

4 Conclusion

In this paper, we have considered flow in heterogeneous porous media made of soluble and insoluble materials. Modeling the dissolution of such a system requires to take into account the multiple scales involved: (i) pore-scale, (ii) Darcy-scale, (iii) the scale of the heterogeneities, (iv) the domain scale (reservoir, aquifer, etc.). This paper addressed the problem of upscaling from Darcy- to large-scale, i.e., the scale of an REV locally representative of the heterogeneous porous medium. A study of the Darcy-scale equations allowed us to discuss the constraint necessary to develop a fully closed Darcy- to large-scale upscaling. Such constraint, characterized by the existence of a dissolution front larger than the heterogeneity scale, is only fulfilled below a critical diffusive Damköhler number for low Péclet numbers and below a critical advective Damköhler number for large Péclet numbers. Even under these conditions, the resulting problem involves coupled Darcy- and

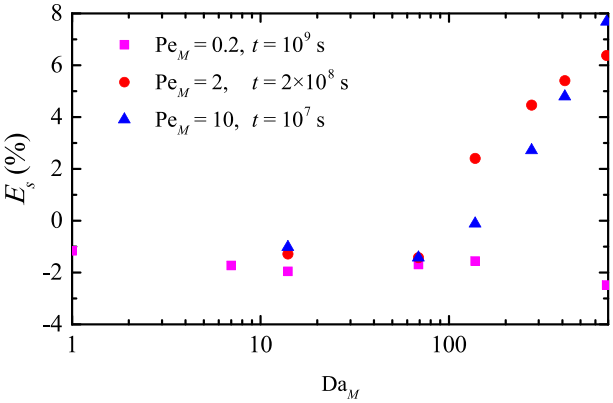

Fig. 10 Relative error in terms of average solid saturation between Darcy- and large-scale models

large-scale equations, and features history effects. However, under the constraints imposed on the Damköhler numbers and assuming that mass exchange coefficients depend only on saturation, it was possible to represent the impact of the dissolution history through a bijective relationship between the Darcy- and large-scale saturation. This allowed to compute *a priori*, before solving actually the large-scale problem, the effective properties needed in the large-scale simulations.

A sequential algorithm was provided to illustrate how to obtain the effective mass exchange coefficient and the effective permeability tensor in the large-scale model, by solving the corresponding closure problems. Large-scale effective parameters were first obtained following the above mentioned algorithm and then used in the large-scale modeling of one stratified and one nodular system. For each system, three Pe_M and various Da_M conditions were considered to investigate the limit of the large-scale model in terms of Da_M and $Da_M Pe_M$. For 1D flow in the stratified system, the large- and Darcy-scale results highly agree with each other, even in the case of high Da_M with sharp dissolution front. This demonstrates the robustness of the large-scale model for such kind of simple systems. This robustness may be attributed to a topological effect: in this 1D case, the flow of the dissolving fluid is forced through all regions, which maintains the same potential for dissolution everywhere in the domain, i.e., no bypassing of slowly dissolving areas. For the nodular system, the results comparisons are also satisfactory in the condition of relatively low Da_M, i.e., when homogenization conditions are fulfilled. When Da_M is large, the large-scale model failed to capture all the details of the Darcy-scale model. Large-scale results give a much thinner dissolution front at similar position compared to the Darcy-scale model, which can be related to the bypassing of slowly dissolving areas.

We addressed the fundamental question of the homogenization conditions to be fulfilled for the construction of a large-scale dissolution model including the effect of Darcy-scale heterogeneities. The computational results validated the large-scale model we developed for the dissolution of porous media with Darcy-scale heterogeneities in the case of a simple dissolution problem. Under these assumptions, two important problems could be resolved: the question of the length-scale separation necessary to develop a fully closed upscaling methodology and historical aspects that prevent some sort of decoupling between the Darcy- and large-scale problems. The good agreement between DNS and large-scale results in the condition of 1D sharp dissolution front is interesting from a fundamental point of view as well as for practical applications. However, limitations of the applicability of the proposed theory must not be overlooked, in particular if one or all constraints are not satisfied. In the paragraph below, we review some of the difficulties that could emerge when departing from the initial dissolution problem considered in this paper.

The case of large Damköhler numbers is obviously the first difficulty. The fact that proper homogenization conditions are not fulfilled does not prevent the system to have some sort of "homogenized" behavior. For instance, heuristic large-scale models have been proposed in the case of 1D large-scale flow for a 2D or 3D core affected by wormhole dissolution (Golfier et al. 2004, 2006). The question of coupling between developing dissolution instabilities and Darcy-scale heterogeneities, which is likely to be very important if the assumption of low Damköhler number is removed, is also largely an open question. Difficulties may arise for the homogenization process, even for low Damköhler numbers, for instance if the mass exchange coefficient depends strongly on velocity. In that case, the decoupling between dissolution and the momentum balance problem is not guaranteed. The case of a multi-component system requires also some attention. Finally, the case of a different driving force to express the Darcy-scale mass exchange term, in particular the reactive case, must also be considered in future work.

Supplementary Information The online version contains supplementary material available at https://doi.org/10.1007/s11242-021-01623-0.

Declarations

Conflict of interest The authors declare that they have no conflict of interest.

References

Abriola, L., Pinder, G.F.: A multiphase approach to the modeling of porous media contaminated by organic compounds -1. Equation development. Water Resour. Res. **21**(1), 11–18 (1985)

Agartan, E., Trevisan, L., Cihan, A., Birkholzer, J., Zhou, Q., Illangasekare, T.H.: Experimental study on effects of geologic heterogeneity in enhancing dissolution trapping of supercritical CO_2. Water Resour. Res. **51**(3), 1635–1648 (2015)

Ahmadi, A., Quintard, M., Whitaker, S.: Transport in chemically and mechanically heterogeneous porous media V: two-equation model for solute transport with adsorption. Adv. Water Resour. **22**(1), 59–86 (1998)

Aris, R.: On the dispersion of a solute in a fluid flowing through a tube. Proceedings of the Royal Society of London. Series A. Mathematical and Physical Sciences **235**(1200), 67–77 (1956)

Banwart, S.A.: Assessing the scale-dependence of mineral weathering rates at the Aitik waste rock deposit in Northern Sweden. Mineral. Mag. **62A**(1), 108–109 (1998)

Békri, S., Renard, S., Delprat-Jannaud, F.: Pore to core scale simulation of the mass transfer with mineral reaction in porous media. Oil Gas Sci. Technol. Revue d'IFP Energies Nouvelles **70**(4), 681–693 (2015)

Békri, S., Thovert, J.F., Adler, P.M.: Dissolution of porous media. Chem. Eng. Sci. **50**, 2765–2791 (1995)

Bourgeat, A.: Homogenized behavior of two-phase flows in naturally fractured reservoirs with uniform fractures distribution. Comput. Methods Appl. Mech. Eng. **47**(1–2), 205–216 (1984)

Bousquet-Melou, P., Neculae, A., Goyeau, B., Quintard, M.: Averaged solute transport during solidification of a binary mixture: active dispersion in dendritic structures. Metall. Mater. Trans. B **33**(3), 365–376 (2002)

Brenner, H., Stewartson, K.: Dispersion resulting from flow through spatially periodic porous media. Philosophical Transactions of the Royal Society of London. Series A, Mathematical and Physical Sciences **297**(1430), 81–133 (1980)

Chabanon, M., Valdés-Parada, F.J., Ochoa-Tapia, J.A., Goyeau, B.: Large-scale model of flow in heterogeneous and hierarchical porous media. Adv. Water Resour. **109**, 41–57 (2017)

Chastanet, J., Wood, B.D.: Mass transfer process in a two-region medium. Water Resour. Res. **44**(5), W05413 (2008)

Chen, L., Kang, Q., Carey, B., Tao, W.: Pore-scale study of diffusion-reaction processes involving dissolution and precipitation using the lattice Boltzmann method. Int. J. Heat Mass Trans. **75**, 483–496 (2014)

Cherblanc, F., Ahmadi, A., Quintard, M.: Two-medium description of dispersion in heterogeneous porous media: calculation of macroscopic properties. Water Resour. Res. **39**(6), 1154 (2003)

Cherblanc, F., Ahmadi, A., Quintard, M.: Two-domain description of solute transport in heterogeneous porous media: Comparison between theoretical predictions and numerical experiments. Adv. Water Resour. **30**(5), 1127–1143 (2007)

Christ, J.A., Lemke, L.D., Abriola, L.M.: The influence of dimensionality on simulations of mass recovery from nonuniform dense non-aqueous phase liquid (DNAPL) source zones. Adv. Water Resour. **32**(3), 401–412 (2009)

Cohen, C., Ding, D., Quintard, M., Bazin, B.: From pore scale to wellbore scale: Impact of geometry on wormhole growth in carbonate acidization. Chem. Eng. Sci. **63**, 3088–3099 (2008)

Cooper, A.: Halite karst geohazards (natural and man-made) in the United Kingdom. Environ. Geol. **42**(5), 505–512 (2002)

Coutelieris, F.A., Kainourgiakis, M.E., Stubos, A.K., Kikkinides, E.S., Yortsos, Y.C.: Multiphase mass transport with partitioning and inter-phase transport in porous media. Chem. Eng. Sci. **61**(14), 4650–4661 (2006)

Dagan, G.: Flow and Transport in Porous Formations. Springer (1989)

Davit, Y., Quintard, M.: Technical notes on volume averaging in porous media I: How to choose a spatial averaging operator for periodic and quasiperiodic structures. Trans. Porous Media **119**(3), 555–584 (2017)
Eidsath, A., Carbonell, R.G., Whitaker, S., Herrmann, L.R.: Dispersion in pulsed systems - III: comparison between theory and experiments for packed beds. Chem. Eng. Sci. **38**(11), 1803–1816 (1983)
Farthing, M.W., Seyedabbasi, M.A., Imhoff, P.T., Miller, C.T.: Influence of porous media heterogeneity on nonaqueous phase liquid dissolution fingering and upscaled mass transfer. Water Resour. Res. **48**(8), W08507 (2012)
Gelhar, L.W., Welty, C., Rehfeldt, K.R.: A critical review of data on field-scale dispersion in aquifers. Water Resour. Res. **28**(7), 1955–1974 (1992)
Golfier, F., B. Bazin, R..L.., Quintard, M.: Core-scale description of porous media dissolution during acid injection - Part I: theoretical development. Comput. Appl. Math. **23**, 173–194 (2004)
Golfier, F., Quintard, M., Bazin, B., Lenormand, R.: Core-scale description of porous media dissolution during acid injection - Part II: calculation of the effective properties. Comput. Appl. Math. **25**, 55–78 (2006)
Golfier, F., Quintard, M., Cherblanc, F., Zinn, B.A., Wood, B.D.: Comparison of theory and experiment for solute transport in highly heterogeneous porous medium. Adv. Water Resour. **30**(11), 2235–2261 (2007)
Golfier, F., Zarcone, C., Bazin, B., Lenormand, R., Lasseux, D., Quintard, M.: On the ability of a Darcy-scale model to capture wormhole formation during the dissolution of a porous medium. J. Fluid Mech. **457**, 213–254 (2002)
Gray, W.G., Leijnse, A., Kolar, R.L., Blain, C.A.: Mathematical Tools for Changing Spatial Scales in the Analysis of Physical Systems. CRC Press, Boca Raton, FL (1993)
Guibert, R., Horgue, P., Debenest, G., Quintard, M.: A comparison of various methods for the numerical evaluation of porous media permeability tensors from pore-scale geometry. Math. Geosci. **48**(3), 329–347 (2016)
Guo, J., Laouafa, F., Quintard, M.: A theoretical and numerical framework for modeling gypsum cavity dissolution. Int. J. Num. Anal.l Methods Geomech. **40**, 1662–1689 (2016)
Guo, J., Quintard, M., Laouafa, F.: Dispersion in porousmedia with heterogeneous nonlinear reactions. Trans. Porous Media **109**(3), 541–570 (2015)
Gvirtzman, H., Paldor, N., Magaritz, M., Bachmat, Y.: Mass exchange between mobile freshwater and immobile saline water in the unsaturated zone. Water Resour. Res. **24**(10), 1638–1644 (1988)
Gwo, J.P., Jardine, P.M., Wilson, G.V., Yeh, G.T.: Using a multiregion model to study the effects of advective and diffusive mass transfer on local physical nonequilibrium and solute mobility in a structured soil. Water Resour. Res. **32**(3), 561–570 (1996)
Hao, Y., Smith, M., Carroll, S.: Multiscale modeling of CO_2-induced carbonate dissolution: from core to meter scale. Int. J. Greenhouse Gas Control **88**, 272–289 (2019)
Hao, Y., Smith, M., Sholokhova, Y., Carroll, S.: CO_2-induced dissolution of low permeability carbonates. part II: numerical modeling of experiments. Adv. Water Resour. **62**, 388–408 (2013)
Kalia, N., Balakotaiah, V.: Modeling and analysis of wormhole formation in reactive dissolution of carbonate rocks. Chem. Eng. Sci. **62**(4), 919–928 (2007)
Kalia, N., Balakotaiah, V.: Effect of medium heterogeneities on reactive dissolution of carbonates. Chem. Eng. Sci. **64**(2), 376–390 (2009)
Kang, Q., Chen, L., Valocchi, A., Viswanathan, H.: Pore-scale study of dissolution-induced changes in permeability and porosity of porous media. J. Hydrol. **517**, 1049–1055 (2014)
Kang, Q., Zhang, D., Chen, S., He, X.: Lattice Boltzmann simulation of chemical dissolution in porous media. Phys. Rev. E **65**, 036318 (2002)
Kitanidis, P.K.: Prediction by the method of moments of transport in a heterogeneous formation. J. Hydrol. **102**, 453–473 (1988)
Laouafa, F., Prunier, F., Daouadji, A., Al Gali, H., Darve, F.: Stability in geomechanics, experimental and numerical analyses. Int. J. Num. Anal. Methods Geomech. **35**(2), 112–139 (2011)
Liu, P., Yan, X., Yao, J., Sun, S.: Modeling and analysis of the acidizing process in carbonate rocks using a two-phase thermal-hydrologic-chemical coupled model. Chem. Eng. Sci. **207**, 215–234 (2019)
Luo, H., Laouafa, F., Guo, J., Quintard, M.: Numerical modeling of three-phase dissolution of underground cavities using a diffuse interface model. Int. J. Num. Anal. Methods Geomech. **38**, 1600–1616 (2014)
Luo, H., Quintard, M., Debenest, G., Laouafa, F.: Properties of a diffuse interface model based on a porous medium theory for solid-liquid dissolution problems. Comput.l Geosci. **16**(4), 913–932 (2012)
Luquot, L., Gouze, P.: Experimental determination of porosity and permeability changes induced by injection of CO_2 into carbonate rocks. Chem. Geol. **265**, 148–159 (2009)
Mabiala, B., Tathy, C., Quintard, M.: NAPL dissolution in heterogeneous systems: Large-scale analysis for stratified system. In: HEFAT 2003, 2nd International Conference on Heat Transfer, Fluid Mechanics and Thermodynamics, vol. paper MB3. Victoria Falls, Zambia (2003)
Marle, C.M.: On macroscopic equations governing multiphase flow with diffusion and chemical reactions in porous media. Int. J. Eng. Sci. **20**(5), 643–662 (1982)

Mei, C.C.: Method of homogenization applied to dispersion in porous media. Trans. Porous Media **9**(3), 261–274 (1992)
Olsson, E., Kreiss, G.: A conservative level set method for two phase flow. J. Comput. Phys. **210**(1), 225–246 (2005)
Olsson, E., Kreiss, G., Zahedi, S.: A conservative level set method for two phase flow II. J. Comput. Phys. **225**, 785–807 (2007)
Panga, M.K.R., Ziauddin, M., Balakotaiah, V.: Two-scale continuum model for simulation of wormholes in carbonate acidization. AIChE J. **51**(12), 3231–3248 (2005)
Parker, J., Park, E.: Modeling field-scale nonaqueous phase dissolution kinetics in heterogeneous aquifers. Water Resour. Res. **40**, W05109 (2004)
Prunier, F., Laouafa, F., Darve, F.: 3D bifurcation analysis in geomaterials: investigation of the second order work criterion. Eur. J. Environ. Civ. Eng. **13**(2), 135–147 (2009)
Prunier, F., Nicot, F., Darve, F., Laouafa, F., Lignon, S.: Three-dimensional multiscale bifurcation analysis of granular media. J. Eng. Mech. **135**(6), 493–509 (2009)
Quintard, M., Whitaker, S.: Ecoulement monophasique en milieu poreux: effet des hétérogénéités locales. J. Theor. Appl. Mech. **6**(5), 691–726 (1987)
Quintard, M., Whitaker, S.: Two-phase flow in heterogeneous porous media: the method of large-scale averaging. Trans. Porous Media **3**, 357–413 (1988)
Quintard, M., Whitaker, S.: Convection, dispersion, and interfacial transport of contaminants: homogeneous porous media. Adv. Water Resources **17**, 221–239 (1994)
Quintard, M., Whitaker, S.: Transport in ordered and disordered porous media I: the cellular average and the use of weighting functions. Trans. Porous Media **14**, 163–177 (1994)
Quintard, M., Whitaker, S.: Dissolution of an immobile phase during flow in porous media. Ind. Eng. Chem. Res. **38**(3), 833–844 (1999)
Renard, P., de Marsily, G.: Calculating equivalent permeability: a review. Adv. Water Resour. **20**(5), 253–278 (1997)
Säez, A.E., Otero, C.J., Rusinek, I.: The effective homogeneous behavior of heterogeneous porous media. Transp. Porous Media **4**, 213–238 (1989)
Sánchez-Vila, X., Girardi, J.P., Carrera, J.: A synthesis of approaches to upscaling of hydraulic conductivities. Water Resour. Res. **31**(4), 867–882 (1995)
Soulaine, C., Roman, S., Kovscek, A., Tchelepi, H.A.: Mineral dissolution and wormholing from a pore-scale perspective. J. Fluid Mech. **827**, 457–483 (2017)
Soulaine, C., Roman, S., Kovscek, A., Tchelepi, H.A.: Pore-scale modelling of multiphase reactive flow: application to mineral dissolution with production of CO_2. J. Fluid Mech. **855**, 616–645 (2018)
Starchenko, V., Marra, C.J., Ladd, A.J.C.: Three-dimensional simulations of fracture dissolution. J. Geophys. Res. Solid Earth **121**(9), 6421–6444 (2016)
Szymczak, P., Ladd, A.J.C.: Instabilities in the dissolution of a porous matrix. Geophys. Res. Lett. **38**, L07403 (2011)
Taylor, G.: Dispersion of soluble matter in solvent flowing slowly through a tube. Proceedings of the Royal Society of London. Series A. Mathematical and Physical Sciences **219**(1137), 186–203 (1953)
Taylor, G.: The dispersion of matter in turbulent flow through a pipe. Proceedings of the Royal Society of London. Series A. Mathematical and Physical Sciences **223**(1155), 446–468 (1954)
Tran Ngoc, T..D., Le, N..H..N., Tran, T..V., Ahmadi, A., Bertin, H.: Homogenization of solute transport in unsaturated double-porosity media: model and numerical validation. Trans. Porous Media **132**(1), 53–81 (2020)
Varloteaux, C., Békri, S., Adler, P.M.: Pore network modelling to determine the transport properties in presence of a reactive fluid: from pore to reservoir scale. Adv. Water Resour. **53**, 87–100 (2013)
Vignoles, G.L., Aspa, Y., Quintard, M.: Modelling of carbon-carbon composite ablation in rocket nozzles. Compos. Sci. Technol. **70**(9), 1303–1311 (2010)
Whitaker, S.: Flow in porous media I: a theoretical derivation of Darcy's law. Trans. Porous Media **1**(1), 3–25 (1986)
Whitaker, S.: The Method of, vol. Averaging. Kluwer Academic Publishers, Dordrecht, The Netherlands (1999)
White, A.F., Brantley, S.L.: The effect of time on the weathering of silicate minerals: Why do weathering rates differ in the laboratory and field? Chem. Geol. **202**(3–4), 479–506 (2003)

Authors and Affiliations

Jianwei Guo[1] · Farid Laouafa[2] · Michel Quintard[3]

[1] School of Mechanics and Engineering, Southwest Jiaotong University, Chengdu 610031, China

[2] National Institute for Industrial Environment and Risks (INERIS), 60550 Verneuil en Halatte, France

[3] CNRS- INPT- UPS, Institut de Mécanique des Fluides de Toulouse (IMFT), Université de Toulouse, 31400 Toulouse, France